SANDIA REPORT
SAND2022-1383
Printed Click here to enter a date

Sandia National Laboratories

Analysis of Experimental Shock Propagation through a Diverse Set of Geometric Cavities Embedded in Lab-Scale Polymer Cubes

James Nelsen, Shuyue Guo, Kirsten Chojnicki

Prepared by
Sandia National Laboratories
Albuquerque, New Mexico
87185 and Livermore,
California 94550

Issued by Sandia National Laboratories, operated for the United States Department of Energy by National Technology & Engineering Solutions of Sandia, LLC.

Available to DOE and DOE contractors from
U.S. Department of Energy
Office of Scientific and Technical Information
P.O. Box 62
Oak Ridge, TN 37831

Telephone: (865) 576-8401
Facsimile: (865) 576-5728
E-Mail: reports@osti.gov
Online ordering: http://www.osti.gov/scitech

Available to the public from
U.S. Department of Commerce
National Technical Information Service
5301 Shawnee Rd
Alexandria, VA 22312

Telephone: (800) 553-6847
Facsimile: (703) 605-6900
E-Mail: orders@ntis.gov
Online order: https://classic.ntis.gov/help/order-methods/

ABSTRACT

Experiments were designed and conducted to investigate the impact that geometric cavities have on the transfer of energy from an embedded explosion to the surface of the physical domain. The experimental domains were fabricated as 3-inch polymer cubes, with varying cavity geometries centered in the cubes. The energy transfer, represented as a shock wave, was generated by the detonation of an exploding bridgewire at the center of the cavity. The shock propagation was tracked by schlieren imaging through the optically accessible polymer. The magnitude of energy transferred to the surface was recorded by an array of pressure sensors. A minimum of five experimental runs were conducted for each cavity geometry and statistical results were developed and compared. Results demonstrated the decoupling effect that geometric cavities produce on the energy field at the surface.

ACKNOWLEDGEMENTS

This research was funded by the National Nuclear Security Administration, Defense Nuclear Nonproliferation Research and Development. The authors acknowledge important interdisciplinary collaboration with scientists and engineers from Los Alamos National Laboratory, Lawrence Livermore National Laboratory, Mission Support and Test Services, Pacific Northwest National Laboratory, and Sandia National Laboratories. This report describes objective technical results and analysis. Any subjective views or opinions that might be expressed in the paper do not necessarily represent the views of the U.S. Department of Energy or the United States Government. The authors are grateful to Marcia Cooper for assisting in the design of the experiments analyzed in this report. The authors also acknowledge the contributions of Michael Hileman for fabricating the polymer cube domains and Mathew Ingraham for measuring the sample cube sound speeds. The authors also recognize the pressure measurements made by Michael Oliver and the considerable contributions of Adam Sapp and Wayne Trott in performing the experiments. The authors also want to recognize the significant input of guidance and editing of this document by Lauren Wheeler and Stephanie Eras. Finally, the authors acknowledge the analysis of the shock wave speeds by Andrew Mihalik.

CONTENTS

LIST OF FIGURES

LIST OF TABLES

This page left blank

ACRONYMS AND DEFINITIONS

Abbreviation	Definition
	There are no acronyms in this report.

1. INTRODUCTION

Correlating the near-field seismic response to an underground chemical explosion requires knowledge of the energy transfer path, among other variables. The energy transfer path is generally heterogenous and may also contain voids. The introduction of voids complicates the signal transfer, and the magnitude of dissipation depends on the size and geometry of the cavity. This investigation isolates the impact of cavity size and diverse geometries on the energy field response of an induced shock wave through a homogeneous domain.

2. EXPERIMENT DESIGN

This report is a follow-on to a previous report, (Chojnicki 2017), which provides a detailed record of the experimental design, equipment, fabrication techniques and sensors used, including a discussion of the schlieren imaging technique. As such, the reader is referred to the previous report for experimental setup details. However, it should be noted that an improvement in the energy field response was implemented after the early results were published in Chojnicki (2017). The initial experiments conducted in 2016 and 2017 used a single pressure transducer. The results published in this report used a pressure transducer array and standardized the contact pressure of the transducer array against the top surface of the optically accessible polymer cubes.

Seventeen different cavity geometries were fabricated and tested for this investigation. Appendix A displays an image of each individual cube with the embedded cavity geometries and relevant geometric properties. Two additional cases were tested: open-air (representing an infinite cavity case) and a no-cavity case (also shown in Appendix A). As observed later, these two non-cavity cases provided limiting bounds, as the open-air represents the completely decoupled case and the no-cavity geometry embodies the completely coupled (also known as tamped) case. To test the consistency in the fabrication technique and the homogeneity of the polymer, a generic, homogeneous cube was tested and demonstrated remarkable consistency in the speed of sound (Chojnicki 2017).

A minimum of five experimental runs were conducted for each of the nineteen different experimental domains, as detailed in Table 1. Current and voltage data were collected to assess the explosive burst energy from the detonated bridgewire, shock tracking to determine the energy transfer velocity, and transient pressure recordings to evaluate the surrogate seismic response. Five experimental runs for each cube domain were selected as a practical limit, although it allowed a simple statistical evaluation of the source energy variability.

Table 1. Details of experiments conducted

Cavity Geometry	Abscissa Number (Figures 5,6,7,15,16)	Cube Name	Date of Experiments	Number of Runs
Air	1		05/22/2018	5
No Cavity	2	Gordon	05/07/2018, 05/23/2018	10
Small Sphere	3	Happy	05/23/2018	5
Medium Sphere	4	Cake	05/09/2018	5
Large Sphere	5	Doc	05/23/2018	5
Small Hemisphere	6	Luna	03/05/2019	6
Medium Hemisphere	7	Hamy	05/09/2018	5
Large Hemisphere	8	Mario	12/17/2018	5
Medium Square	9	Draco	03/05/2019, 03/06/2019	7
Ovoid 1	10	Hermione	03/05/2019	5
Ovoid 2	11	Ron	03/05/2019	5

Cavity Geometry	Abscissa Number (Figures 5,6,7,15,16)	Cube Name	Date of Experiments	Number of Runs
NonSymmetric 1	12	Pumpkin	03/07/2019	5
NonSymmetric 2	13	Voldy	03/06/2019	5
Single Exit Pipe, Short Length,	14	Lilith	06/04/2019	5
Single Exit Pipe, Long Length,	15	Lambda	06/04/2019	6
Dual Exit Pipe, Short Length, Small Diameter	16	LT	04/15/2019	6
Dual Exit Pipe, Long Length, Small Diameter	17	Tau	04/16/2019	5
Dual Exit Pipe, Short Length, Large Diameter	18	IceTea	04/16/2019	5
Dual Exit Pipe, Long Length, Large Diameter	19	Mr.T	04/16/2019	5

2.1. Burst Energy Result

The bridgewire was located on the top surface of a pedestal and centered in the geometric cavity, as shown in Figure 1. The burst energy resulting from the detonation of the bridgewire is calculated as the current times voltage integrated over time (referenced as cumulative energy) until a short is achieved in the circuit (generally a precipitous drop-off in the voltage). Figure 2 exhibits an example of the current trace and Figure 3 an example of the simultaneous voltage trace. Figure 4 displays both the instantaneous energy and cumulative energy for a sample run. In general, the burst energy was achieved in less than 1 microsecond for all runs.

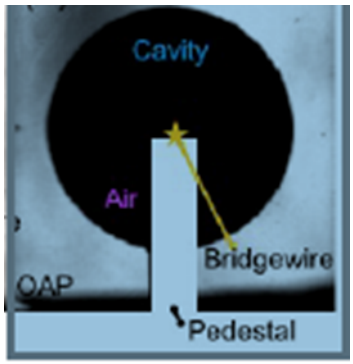

Figure 1. Bridgewire location in cavity geometry

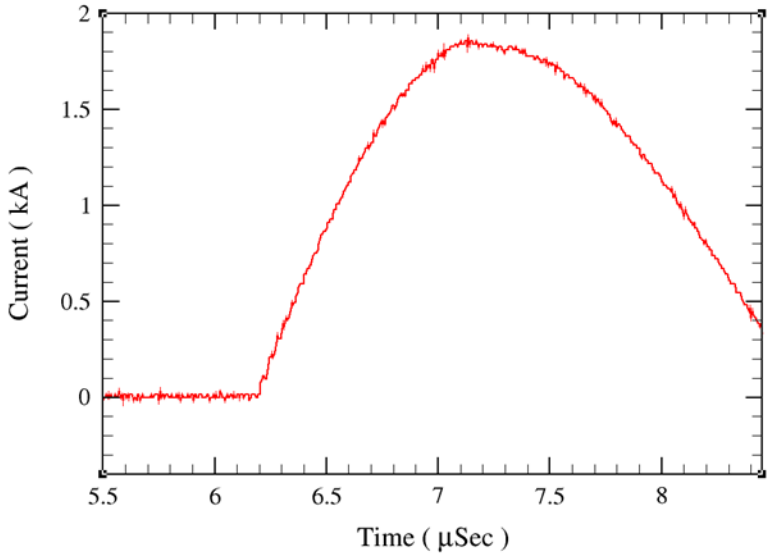

Figure 2. Instantaneous current trace

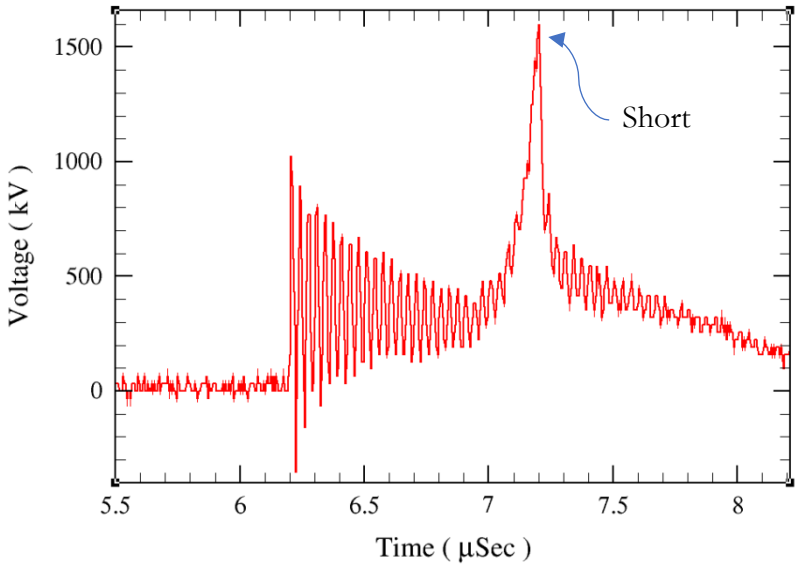

Figure 3. Instantaneous voltage trace

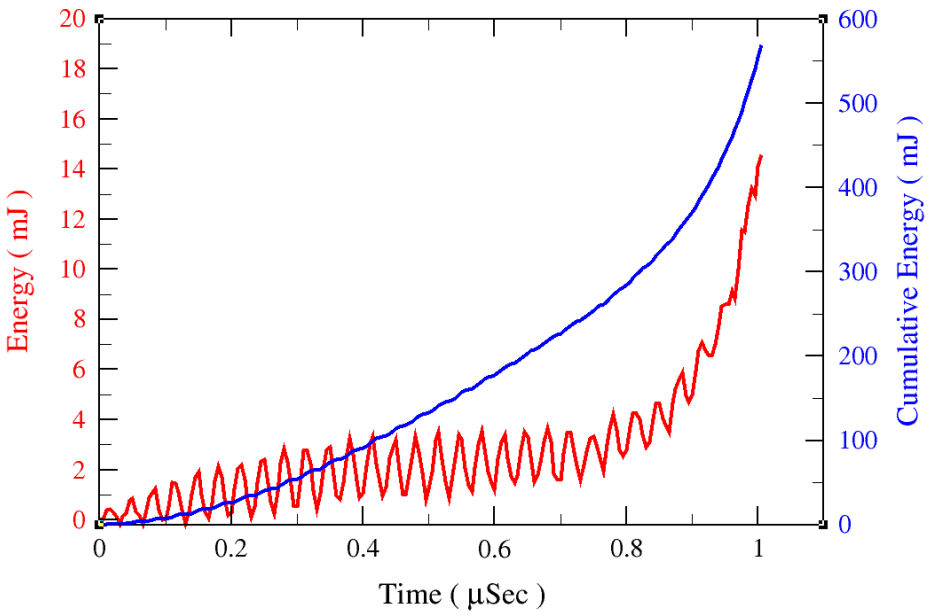

Figure 4. Instantaneous and cumulative burst energy

Ideally, the burst energy would be constant for all the experimental runs such that the exclusive variable being tested would be the cavity geometry. Intuitively, a higher burst energy would produce a stronger shock, leading to an increase in the seismic response at the pressure sensors. As previously stated, the variability of the burst energy was explored with the introduction of a minimum of five experimental runs for each cavity geometry. Figure 5 exhibits the mean burst energy and one standard deviation from the mean for all nineteen experimental geometries. Table 1 provides the details of the specific cavity geometry (correlated to the abscissa number). All the cavity geometries are listed in Table 1 and exhibited in Appendix A, with their void dimensions. In addition, a statistical analysis was conducted on all the burst energy experimental runs, resulting in a mean value of 590 mJ and a standard deviation of 52 mJ. This demonstrates a standard deviation less than 9% of the mean, which supports the desired outcome that the experimental explosion source and data acquisition system is well controlled. Spatial variations in the energy field at the cube surface can therefore be attributed to variations in the path of the wave, which in these experiments is caused by variations in cavity shape.

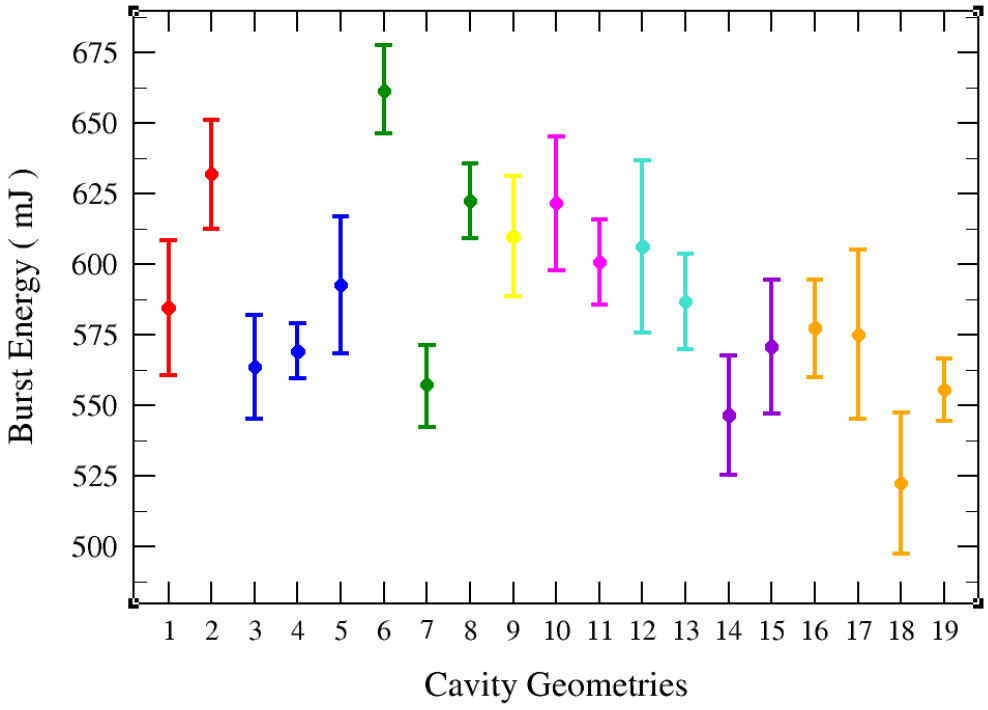

Figure 5. Mean burst energy and one standard deviation for all cavity geometries. The color scheme groups similar geometries: red for the two bounding cases, blue for the spherical cavities, green for the hemispherical cavities, yellow for the box cavity, magenta for the ovoid cavities, turquoise for the nonsymmetrical cavities, violet for the single exit pipe cavities and orange for the dual exit pipe cavities.

As a final check of consistency, the previously stated intuitive hypothesis is explored. That is, for a given set of experimental data, is there a correlation between burst energy, shock speed and pressure sensor response? For this examination, the no-cavity geometry was selected such that the cavity geometry did not influence the results. The data is presented in Table 2 for five experimental runs using the no-cavity geometry. Certainly, the correlation is not definitive, however, there are trends that support intuition. For example, Run 1 has the largest burst energy and the highest shock speed, but inexplicably the lowest peak pressure. Further, Run 3 has the second highest burst energy, the second highest shock speed and the highest peak pressure.

Table 2. Consistency check of variables for no-cavity geometry

Experimental Run	Burst Energy (mJ)	Shock Speed (m/s)	Peak Pressure (MPa)
1	686.1	1055	0.79
2	613.3	1034	0.96
3	668.1	1036	1.00
4	607.4	1022	0.96
5	585.1	1033	0.89

2.2. Shock Velocity Results

The shock velocity through the polymer was computed using images captured by the schlieren camera system. As noted in Chojnicki (2017), the schlieren technique detects density variations in the optically accessible polymer, allowing an exemplary method for tracking the shock wave. The camera system was operated at 500 kHz, with each image capturing a 2 mm progression of the evolving shock wave traveling at an average velocity of 1000 m/s (as an example). The image analysis software is not autonomous, however, as the analyst must specify several parameters to produce a best fit to the shock front. Consequently, it is acknowledged that the shock speed is somewhat subjective, and a parameter estimation uncertainty analysis led to a variation of approximately 2% in shock speed magnitude.

Similar to the burst energy results, the shock velocity results are presented in Figure 6, referencing Table 1 again for the specific cavity geometry. The first observation is that the results for air are not exhibited on the plot. The speed of the induced shock wave through air was detailed in Chojnicki (2017) as 524.5 m/s with a standard deviation of 3.5 m/s. As expected, the speed of the shock through a gas is significantly slower than the speed of the shock through a solid. To demonstrate this stark difference, the shock velocity through air has been added to the plot and the combined result is exhibited in Figure 7. Two significant conclusions can be deduced from Figure 6. First, the shock velocity means are relatively similar in magnitude, with less than a 5% spread for 17 of the 18 geometries plotted. A general conclusion from this observation is that the shock speed through the polymer is relatively insensitive to the burst energy, at least within the range of energies achieved in this test series. The single out-of-family result is for the Ovoid2/"Ron" cavity geometry (label #11), although its mean is less than 4% below the low end of the in-family results. Second, the standard deviations are quite small, with the largest being less than 3% of the mean (label #9, Medium Square/"Draco" cavity) and the smallest being virtually zero (label #18, Dual Exit Pipe, Short Length, Large Diameter/"Ice Tea").

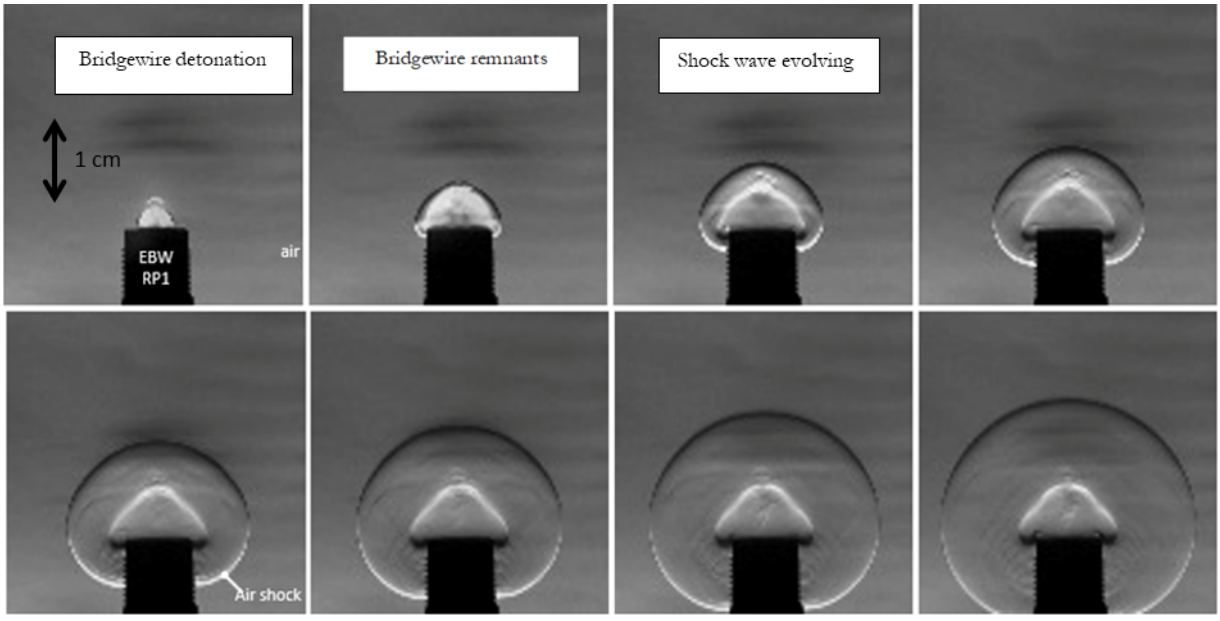

Figure 8 exhibits a series of time-elapsed schlieren photos that demonstrate the evolution of the shock wave in open air. The top left photo shows the early time bridgewire explosion, followed by the evolving conical remnants of the bridgewire (atomized gold), proceeding to the spherical shock

wave progression. The pedestal clearly interferes with the spherical evolution of the shock wave below the pedestal, but all the instrumentation is topside, which experiences a clean, spherical shock wave.

Finally, it is instructive to recall from Chojnicki (2017) that the shock waves are not always symmetric. Figure 9 demonstrates a symmetric shock wave, while Figure 10 exhibits a non-symmetric shock wave. The potential sources of the asymmetry are discussed in the previous report and it is noted that asymmetry will impact the pressure transducer results discussed in the next section.

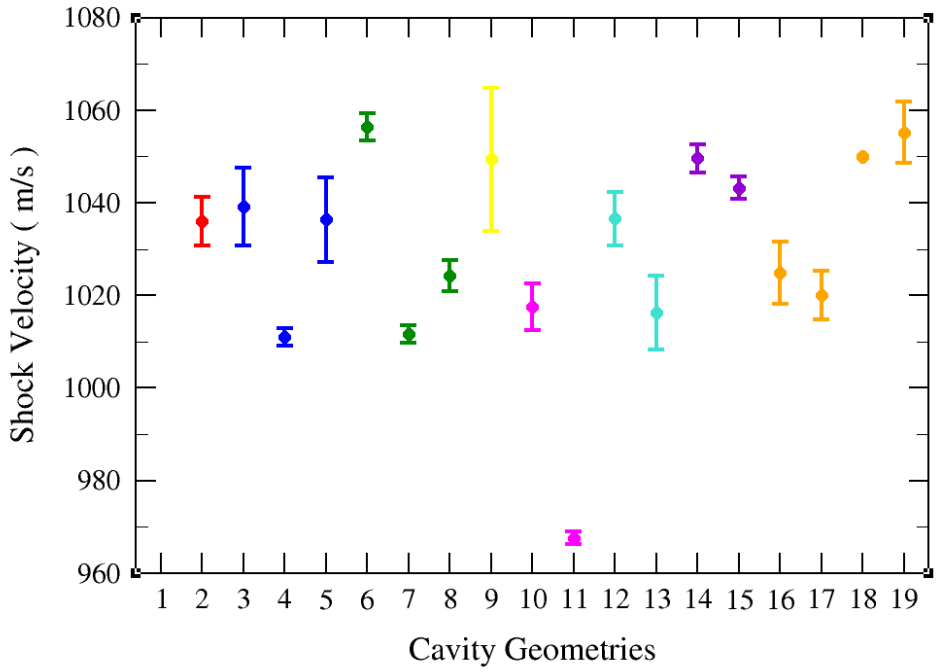

Figure 6. Mean shock velocity and one standard deviation for all cavity geometries

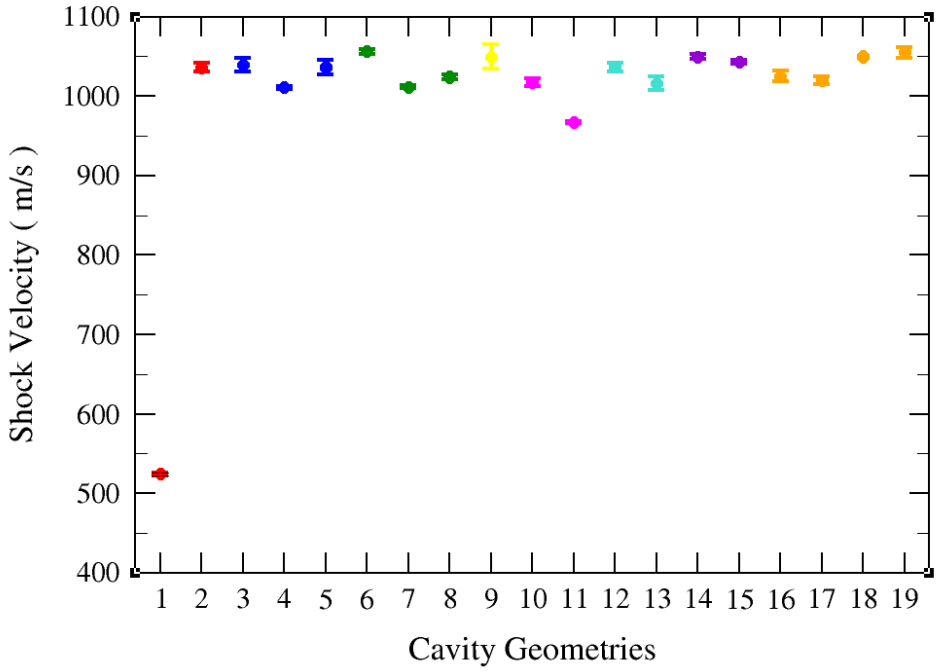

Figure 7. Figure 6 results with shock velocity through air results appended

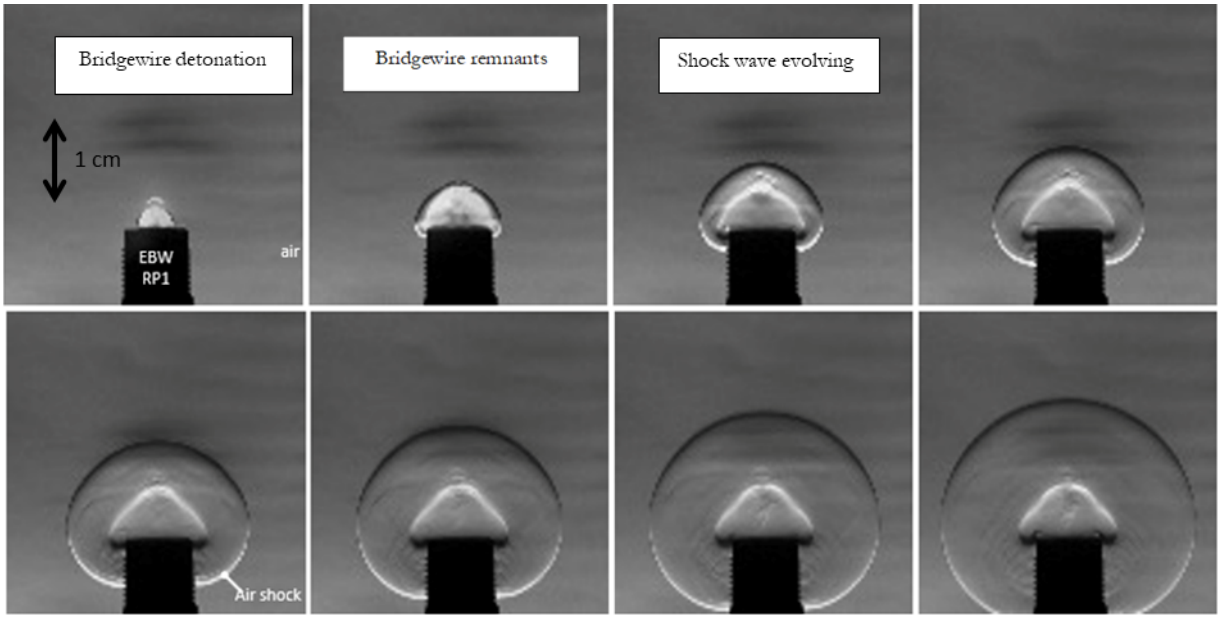

Figure 8. Shock wave evolution in open air.

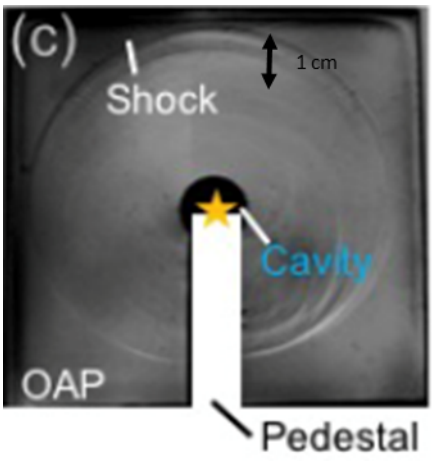

Figure 9. Symmetric spherical shock wave progression from small spherical cavity

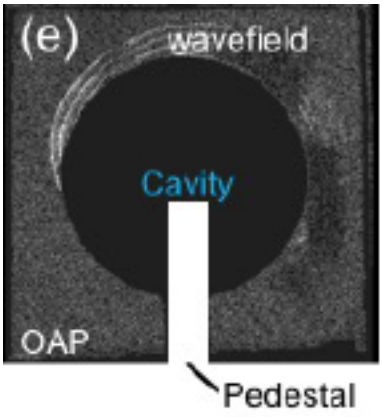

Figure 10. Asymmetric spherical shock wave progression from large spherical cavity

2.3. Surface Pressure Response Results

The surrogate seismic response to the shock wave was provided by an array of pressure transducers mounted to the top surface of the cube domains. Figure 11 portrays the sensor array sequence on the top of the cube. As shown, the transducer at position 1 (center of the top surface) will always exhibit the first response to a symmetric shock wave emanating from the center of a cavity and hence the peak pressure. The behavior of the shock wave at this location is the focus of this report.

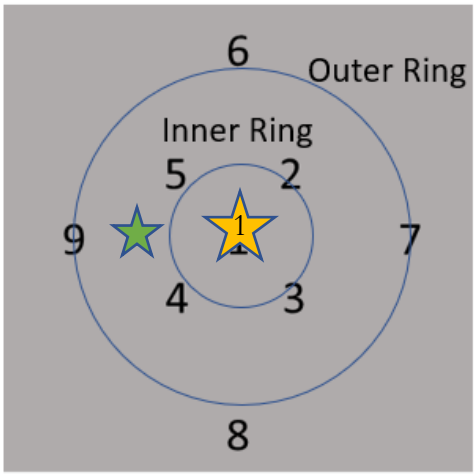

Figure 11. Pressure transducer array on the top of cube.

Figure 12 through Figure 14 exhibit transient pressure traces for two of the cavity geometries and open air. Figure 12 shows the trace for open air, Figure 13 represents the symmetric cavities and Figure 14 the pipe cavities. Each color in the figures represents a different experimental run for that distinct geometry. While Sensor 1 data are shown for Figure 12 and Figure 13, Sensor 5 data are shown in Figure 14. The bridgewire was located directly under Sensor 1 (gold star in Figure 11) for most of the experiments, except for the single exit tubular cavity cases (green star in Figure 11). For the single exit tubes, peak pressures were observed from transducers 4, 5, and 9, which is why Sensor 5 is shown in Figure 14 to compare with the Sensor 1 data in Figure 12 and Figure 13. First, as noted in Chojnicki (2017), the small spike exceeding the noise level toward the beginning of the trace is the electronic noise generated by the initiation of the exploding bridgewire, and therefore represents a timing fiducial. Using the fiducial, notice the delay in the peak pressure response for the open-air case compared to the cavity cases. This is expected based on the slower shock wave speed in air versus the shock speed in the polymer. Also, notice the similarity in the waveform structures for all runs in each geometry, confirming repeatability of individual experimental runs. Finally, the pressure traces in the cavity geometries exhibit late-time secondary peaks, accounting for the reflected shock waves from the cube and cavity boundaries.

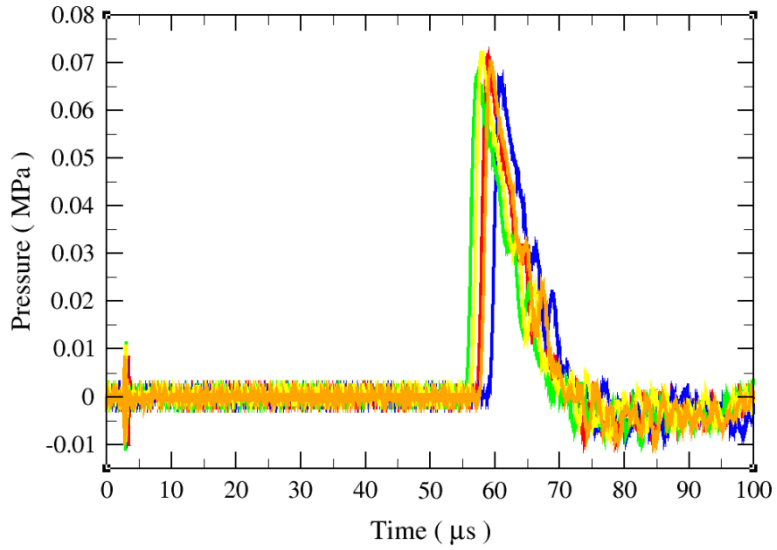

Figure 12. Transient pressure traces for air, Sensor 1. Each color trace represents one of the five experiments.

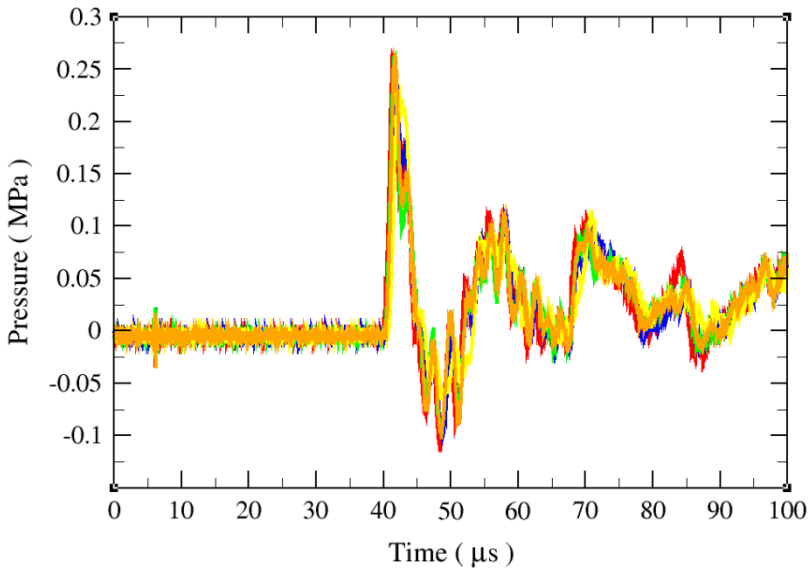

Figure 13. Transient pressure traces for the small hemispherical case ("Luna"), Sensor 1. Each color trace represents one of the six experiments

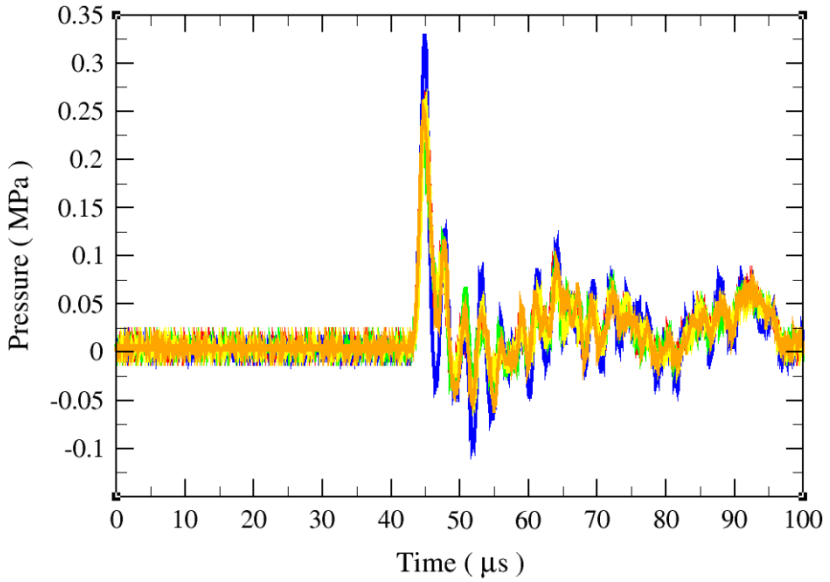

Figure 14. Transient pressure traces for the single-exit pipe, long length pipe case ("Lambda"), Sensor 5. Each color trace represents one of the six experiments.

Similar to the burst energy and shock wave speeds, the composite peak pressures are presented in **Error! Reference source not found.** in a similar format as means and one standard deviation for all of the cavity geometries, including the open-air and no-cavity cases. Figure 15 underscores the decoupling effect of the cavity geometries. The no-cavity case (label 2 on the horizontal axis of the plot) is excluded from Figure 16 as it is significantly larger than the magnitudes of the other cavities and compresses the results. Referencing Figure 16, it is clear that peak pressure is inversely correlated with cavity size (spherical cavities labeled 3 through 5 and hemispherical cavities labeled 6 through 8, progressing from smaller to larger volumes and larger to smaller peak pressures for each geometry). This is certainly the progression of the decoupling effect on display. Even the ellipsoid cavities produce expected results as the horizontal ovoid (Ovoid 1/"Hermione," label 10) achieves a higher pressure than the vertical ovoid (Ovoid 2/"Ron," label 11), demonstrating the shorter path through the polymer produces lower pressures. The pipe structure results are also consistent, as the single and dual exit pipes (labels 14, 15, 16 and 17) with smaller pipe diameters exhibited higher peak pressures than the dual exit pipes (labels 18 and 19) with the larger pipe diameters. It is conjectured that the lower pressures exhibited by the single exit pipes (labels 14 and 15) compared to the dual exit pipes (labels 16 and 17) with identical pipe diameters results from the pedestal offset of the single exit pipe from the center of the cube, which allows destructive interference of the primary shock wave from the reflected shock at the near wall, as shown in Figure 17.

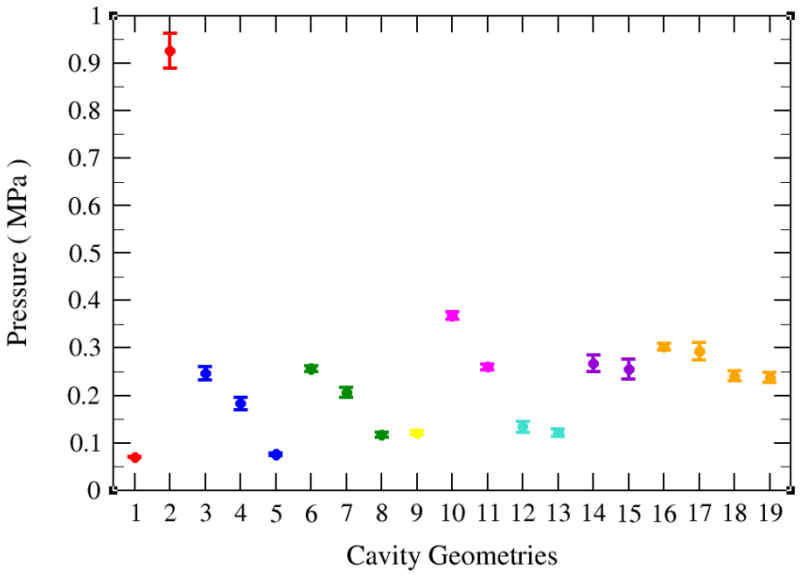

Figure 15. Mean peak pressures and one standard deviation for all cavity geometries including the no-cavity case

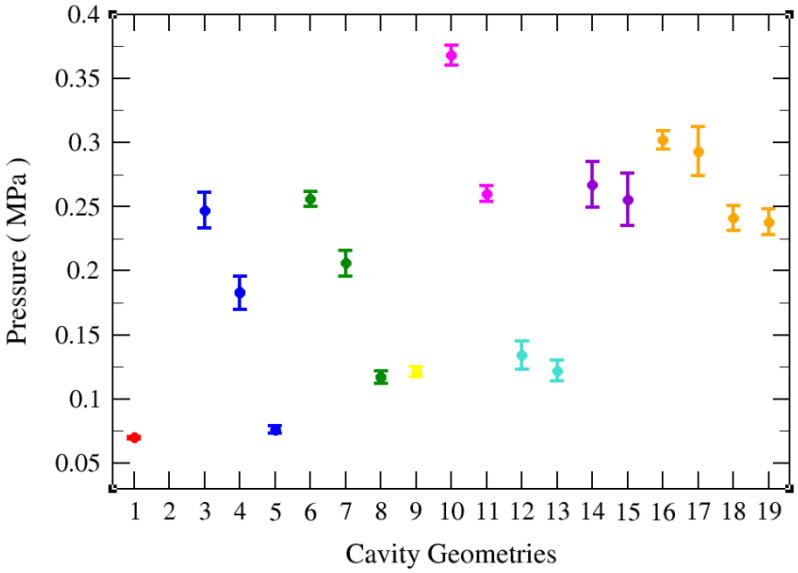

Figure 16. Mean peak pressures and one standard deviation for all cavity geometries, excluding the no-cavity case

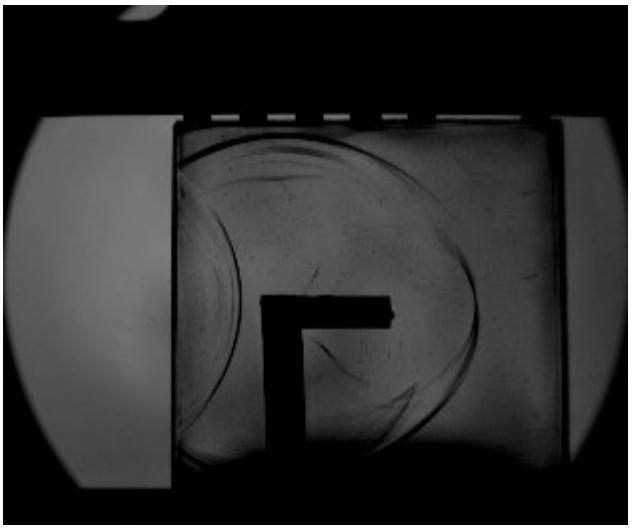

Figure 17. Reflected shock wave from near wall for the single-exit, short length pipe case ("Lilith") representing an offset pedestal case

Finally, the array of pressure transducer results is reviewed for several of the cavity geometries. Figure 18 exhibits the results for the open-air case. As expected, Sensor 1 responds first, followed by the inner ring and the outer ring. The magnitudes are also appropriate as the center sensor (Sensor 1) manifests the highest pressure, followed by the inner ring transducers and the outer ring. It should be observed that the shock wave is reasonably symmetric as the four inner ring sensor responses are nearly indistinguishable, while the four outer ring sensor responses exhibit arrival time differences of a few microseconds and the peak magnitudes are comparable.

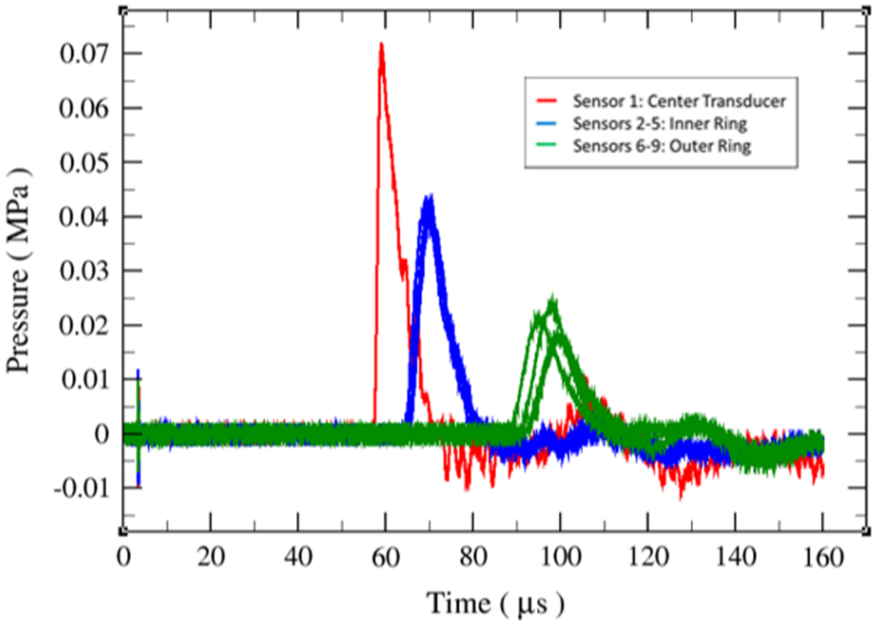

Figure 18. Pressure transducer results for the open-air case

The next case considered is the no-cavity geometry ("Gordon"), presented in Figure 19. Again, the timing is appropriate as the center transducer responds first, followed by the inner and outer ring.

However, note that the response times are compressed compared to the open-air case, affirming the faster shock wave speed in the polymer. Finally, there is very little dissipation of energy between the center transducer and the inner ring as they exhibit identical peak magnitudes and response times differing by only a couple of microseconds.

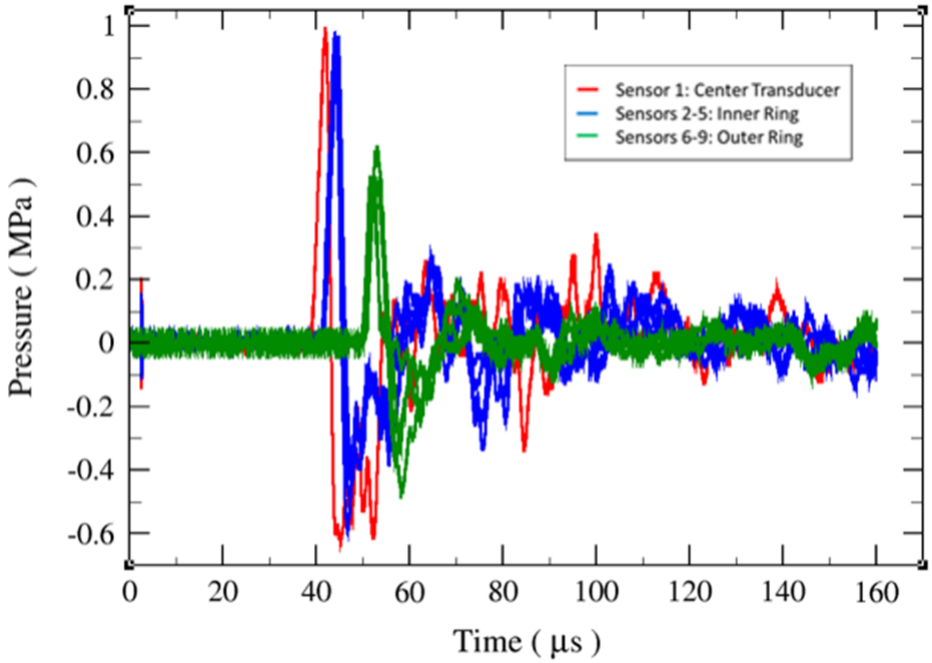

Figure 19. Pressure transducer results for the no-cavity case ("Gordon")

The large spherical cavity results ("Doc") are presented in Figure 20 representing the symmetric cavity geometries. The arrival times and peak pressure magnitudes for the sensor array are as expected. Again, the tight formation of the responses at the inner ring reflects the progression of a symmetrical shock wave that begins to breakdown slightly at the outer ring sensors. As noted previously, the secondary peaks capture the reflected shock waves from the cube boundaries. Also of interest is the magnitude of the peak pressures that are very similar to the open-air case. This observation reinforces the concept that the large cavity has essentially decoupled the explosion from the solid medium. Figure 21 discloses the results for a representative asymmetric single-exit pipe cavity geometry ("Lilith"). The pedestal for Lilith is positioned off-center, closer to the inner and outer ring transducers than the center sensor (see green star in Figure 11). This is reflected in the arrival times and peak magnitudes for the sensor array as the inner and outer ring transducers respond quicker and with greater magnitude than the center transducer. Also observe the relative reduction of the secondary peak amplitudes, a plausible result of the destructive interference of the asymmetric reflected waves.

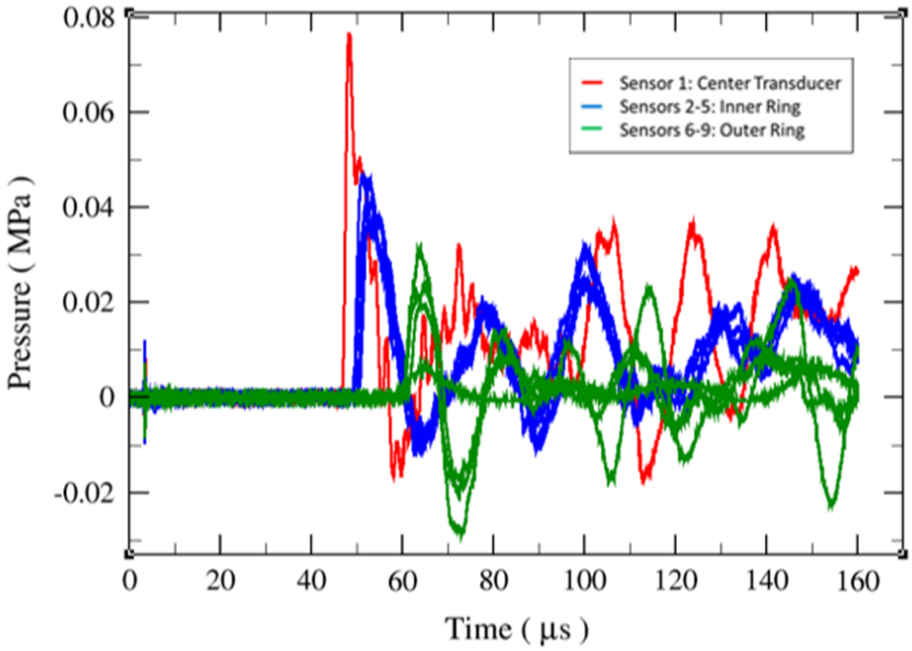

Figure 20. Pressure transducer results for the large spherical cavity ("Doc").

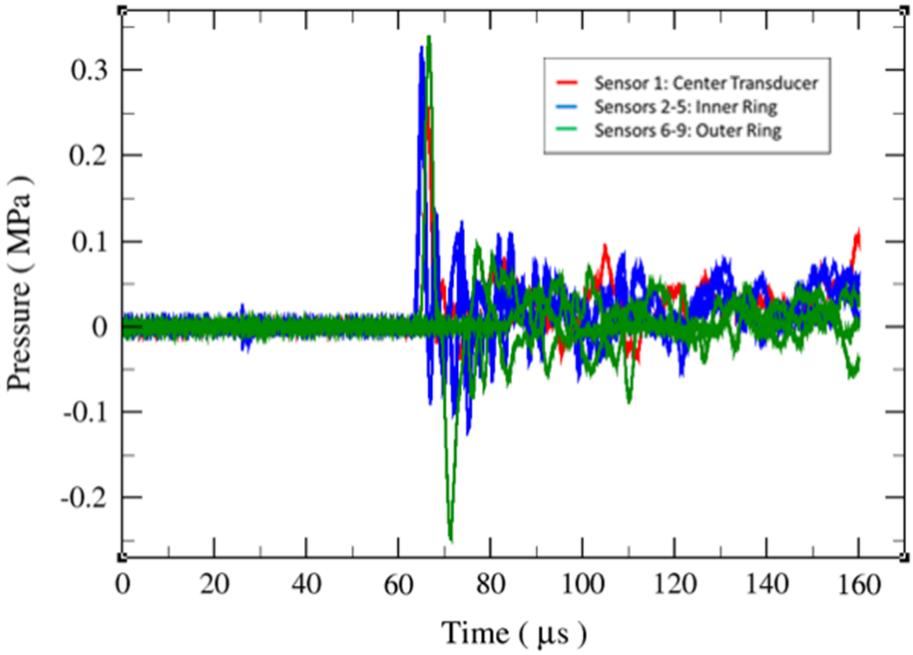

Figure 21. Pressure transducer results for the single-exit, short length pipe cavity ("Lilith")

Results for a representative small-diameter dual-exit pipe cavity geometry ("LT") are presented in Figure 22. Restoring the symmetric position of the pedestal reestablished the expected sensor arrival times and trend in peak pressure magnitudes. The peak pressure magnitudes are noted to be slightly higher than the single-exit pipe cavity results. This is likely because the bridgewire was located

directly under sensor 1 in Figure 22 whereas the bridgewire was not directly located under a sensor when the pedestal was offset in Figure 21.

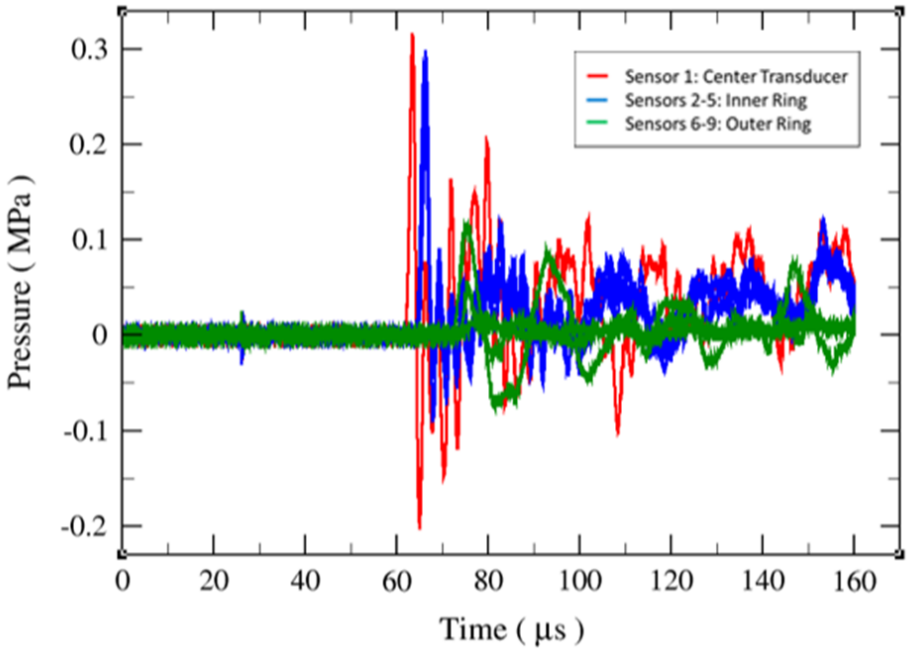

Figure 22. Pressure transducer results for the dual-exit, short length, small-diameter pipe cavity ("LT")

For comparison, the large-diameter dual-exit pipe cavity geometry ("MrT") results are presented in Figure 23. Again, the order of arrival times and trend in peak pressure magnitudes are as expected. Also, as expected, the peak pressure magnitudes are slightly lower than those for the small diameter dual exit cavities, reflecting the presence of the larger cavity, which typically decreases the coupling effect to the solid medium. Finally, a nonsymmetric cavity geometry ("Voldy") results are presented in Figure 24. It appears that the center transducer still manifests the initial response, however the subsequent sensor traces are more chaotic, which is consistent with the highly irregular cavity geometry. Further, the peak pressure magnitudes are significantly lower, supporting the concept of signal suppression using irregular cavity geometries.

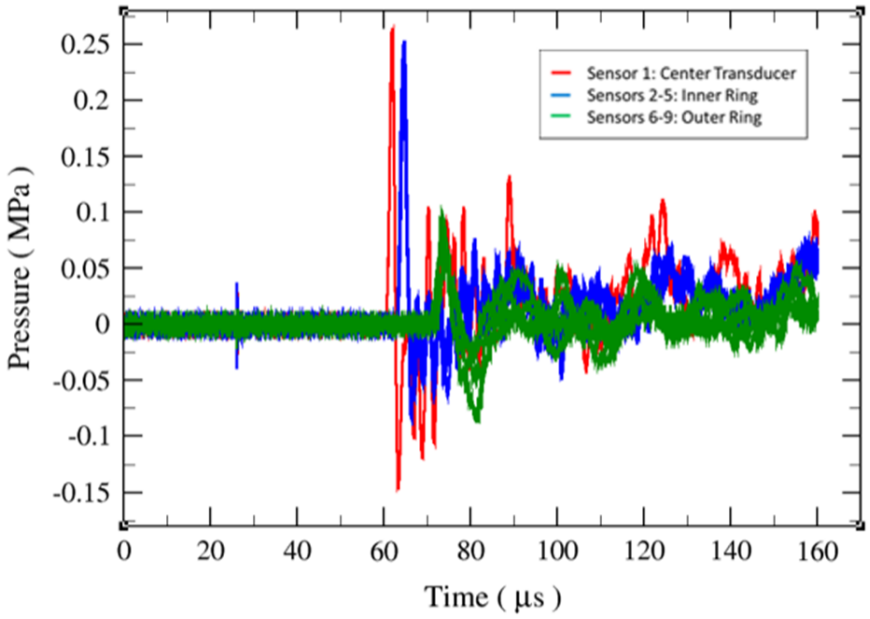

Figure 23. Pressure transducer results for the dual-exit, large-diameter pipe cavity ("IceTea")

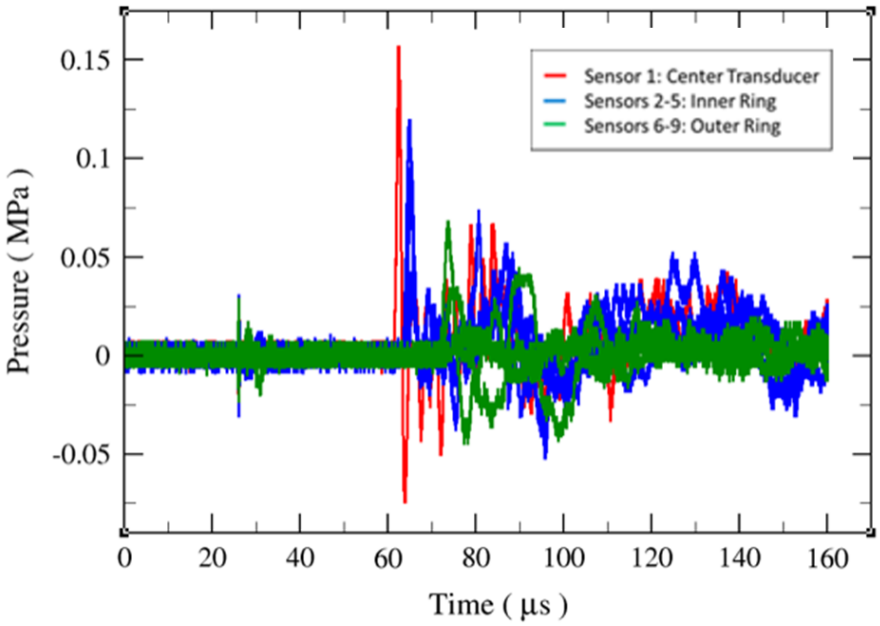

Figure 24. Pressure transducer results for a nonsymmetric cavity ("Voldy")

The balance of the pressure array plots is presented in Appendix B for completeness. The pressure array results are consistent with the summaries described previously.

3. DATA MANAGEMENT

Interested readers may contact the authors for data, which are archived in an SNL repository.

4. SUMMARY

Approximately 100 lab-scale experiments were conducted to assess the influence of different cavity geometries on the propagation of an induced shock wave through a homogeneous polymer. In addition to the 17 cavity geometries explored, two bounding cases were included: open-air and a no-cavity case. Data was acquired from the experiments on the exploding bridgewire energy, the shock wave trajectory and speed, and the surrogate seismic response employing a nine-sensor pressure transducer array. A minimum of five experimental runs were conducted for each of the 19 experimental configurations. Statistical analysis of the explosive energy demonstrated a relatively small standard deviation, thereby permitting a reasonable comparison of the influence of the cavity geometries. The optically accessible polymer used in the fabrication of the scale-model cubes provided an exceptional experimental domain for both the homogeneous material properties and the study of the shock wave trajectories.

The surrogate seismic response at the cube surface, provided by the pressure transducer array, generally followed intuitive and expected results. That is, larger cavities generally manifested smaller surface pressure peak magnitudes, reinforcing the concept of decoupling an explosion from the solid medium. Further, asymmetric cavities can also reduce the propagating energy wave by introducing destructive reflecting waves in the cavity and at the boundaries of the polymer medium.

APPENDIX A. CAVITY GEOMETRIES

Note: Cavity dimensions are based on manufactured positive/male molds and may vary slightly in the actual cube voids. The cavity volumes were determined experimentally using tap water and weighing the cubes before and after the filling of the voids, using standard tap water density.

No Cavity Geometry

Cube Name: Gordon

Cavity Dimensions: Minimum void from contact with bridgewire on top of pedestal.
Cavity Volume: 0.17 ml

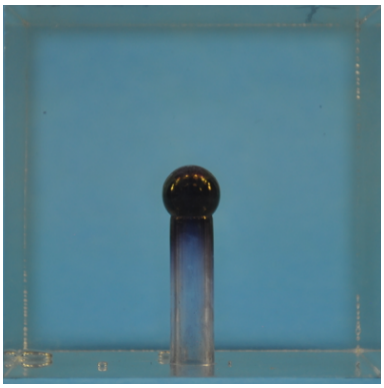

Small Spherical Cavity

Cube Name: Happy

Cavity Dimensions: Centered sphere with radius of 0.25 inches (0.64 cm).
Cavity Volume: 1.14 ml

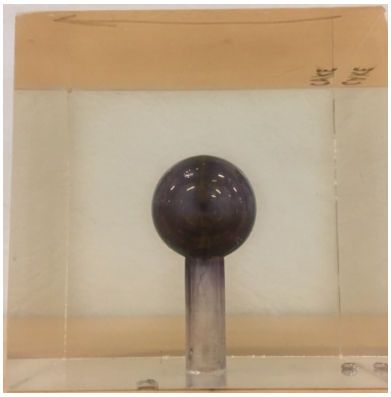

Medium Spherical Cavity

Cube Name: Cake

Cavity Dimensions: Centered sphere with radius of 0.5 inches (1.27 cm).
Cavity Volume: 8.17 ml

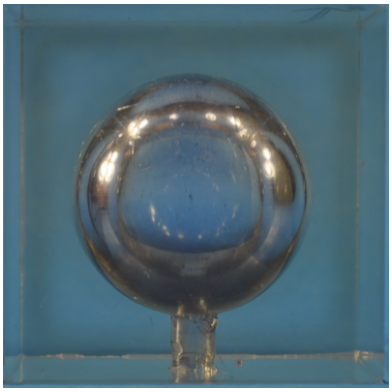

Large Spherical Cavity

Cube Name: Doc

Cavity Dimensions: Centered sphere with radius of 1.0 inches (2.54 cm).
Cavity volume: 70.3 ml

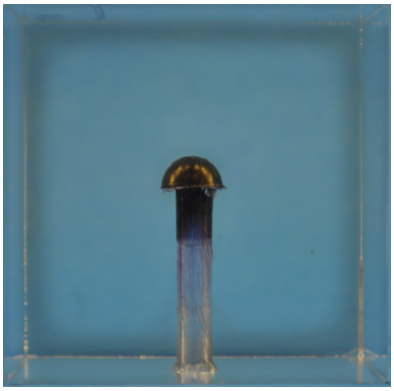

Small Hemispherical Cavity

Cube Name: Luna

Cavity Dimensions: Centered hemisphere with radius of 0.25 inches (0.64 cm).
Cavity Volume: 1.05 ml

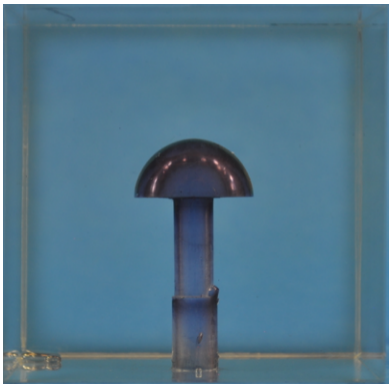

Medium Hemispherical Cavity

Cube Name: Hamy

Cavity Dimensions: Centered hemisphere with radius of 0.5 inches (1.27 cm).
Cavity Volume: 4.03 ml

Large Hemispherical Cavity

Cube Name: Mario

Cavity Dimensions: Centered hemisphere with radius of 1.0 inches (2.54 cm).
Cavity Volume: 36.37 ml

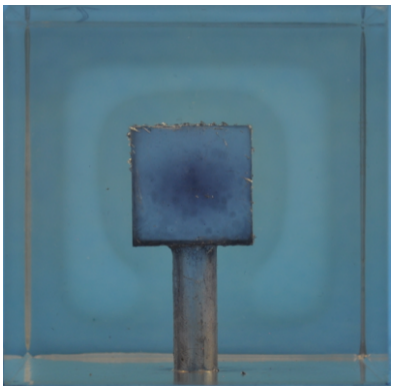

Medium Square Cavity

Cube Name: Draco

Cavity Dimensions: Centered cube with side of 1.0 inches (2.54 cm).
Cavity Volume: 15.24 ml

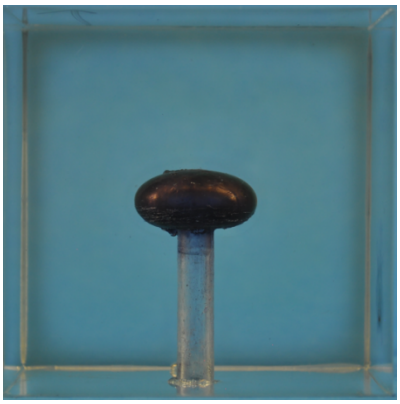

Ovoid1 Cavity

Cube Name: Hermione

Cavity Dimensions: Centered horizontal ellipsoid with minor diameter of 0.48 inches (1.22 cm) and major diameter of 1.00 inches (2.54 cm).
Cavity Volume: 4.48 ml

Ovoid2 Cavity

Cube Name: Ron

Cavity Dimensions: Centered vertical ellipsoid with minor diameter of 0.5 inches (1.27 cm) and major diameter of 0.85 inches (2.16 cm).
Cavity Volume: 2.08 ml

Nonsymmetric1 Cavity

Cube Name: Pumpkin

Cavity Dimensions: Centered medium sphere of radius 0.5 inches (1.27 cm) with superimposed gore bulges.
Cavity Volume: 13.96 ml

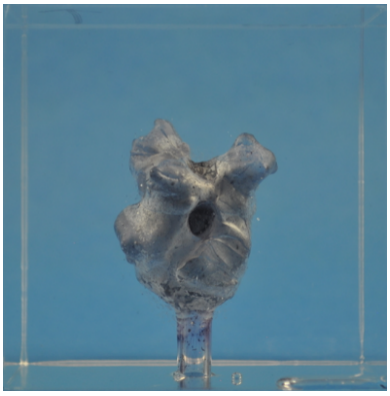

Nonsymmetric2 Cavity

Cube Name: Voldy

Cavity Dimensions: Similar to medium sphere with various concavities and protrusions.
Cavity Volume: 13.2 ml

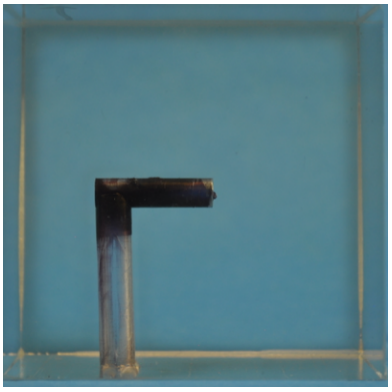

Single-Exit Pipe, Short Length Cavity

Cube Name: Lilith

Cavity Dimensions: Tube structure with diameter 0.25 inches (0.64 cm) and length 1.0 inches (2.54 cm)
Cavity Volume: 0.95 ml

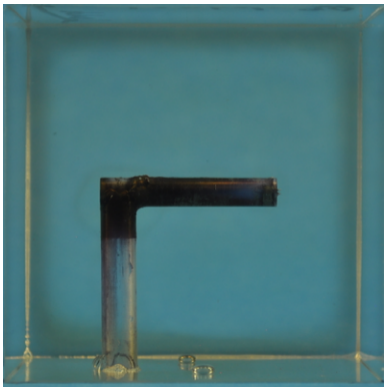

Single-Exit Pipe, Long Length Cavity

Cube Name: Lambda

Cavity Dimensions: Tube structure with diameter 0.25 inches (0.64 cm) and length 1.5 inches (3.81 cm).
Cavity Volume: 1.54 ml

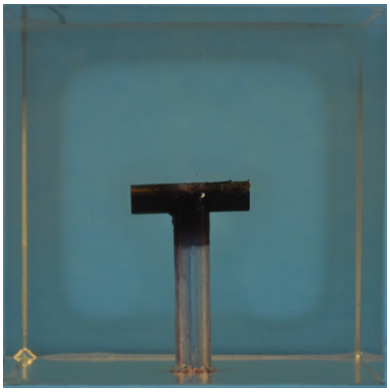

Dual-Exit Pipe, Short Length, Small Diameter Cavity

Cube Name: LT

Cavity Dimensions: Tube structure with diameter 0.25 inches (0.64 cm) and length 1.0 inches (2.54 cm).
Cavity Volume: 1.15 cm^3

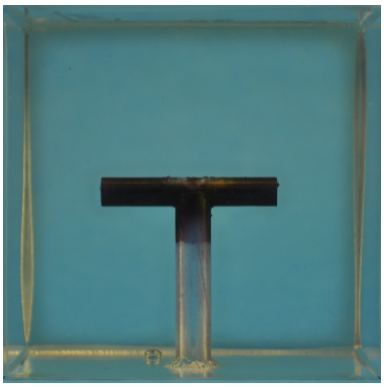

Dual-Exit Pipe, Long Length, Small Diameter Cavity

Cube Name: Tau

Cavity Dimensions: Tube structure with diameter 0.25 inches (0.64 cm) and length 1.5 inches (3.81 cm).
Cavity Volume: 1.06 c^3.

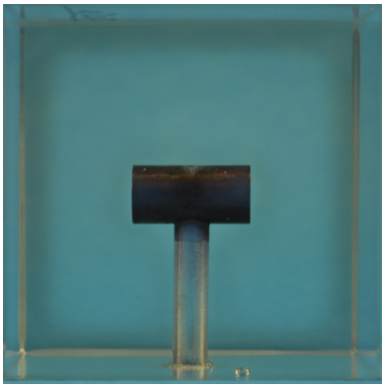

Dual-Exit Pipe, Short Length, Large-Diameter Cavity

Cube Name: Ice Tea

Cavity Dimensions: Tube structure with diameter 0.5 inches (1.27 cm) and length 1.0 inches (2.54 cm).
Cavity Volume: 3.09 cm^3

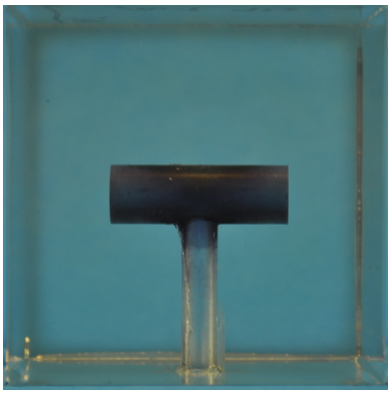

Dual-Exit Pipe, Long Length, Large-Diameter Cavity

Cube Name: Mr. T

Cavity Dimensions: Tube structure with diameter 0.5 inches (1.27 cm) and length 1.5 inches (2.54 cm).
Cavity Volume: 4.85 cm^3

APPENDIX B. CAVITY PRESSURE ARRAY RESULTS

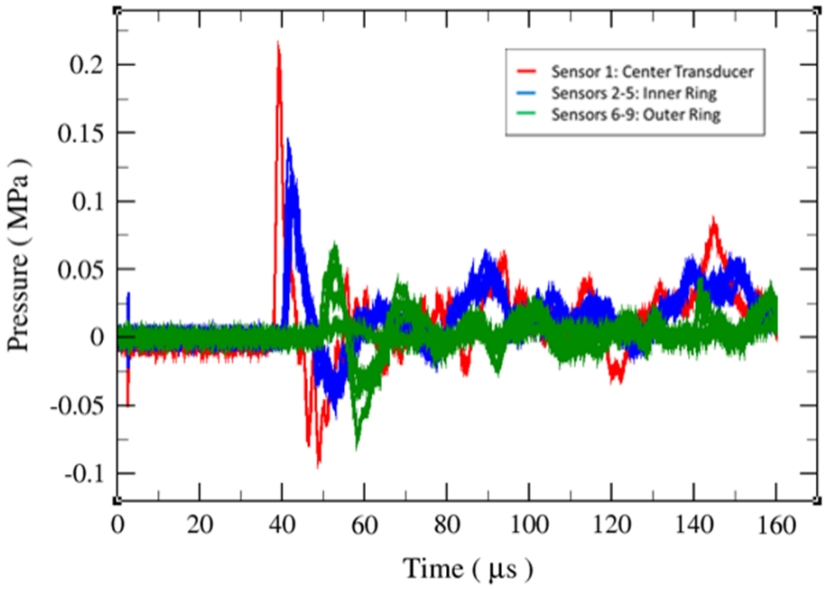

Figure B25. Pressure transducer results for the medium spherical cavity (Cake)

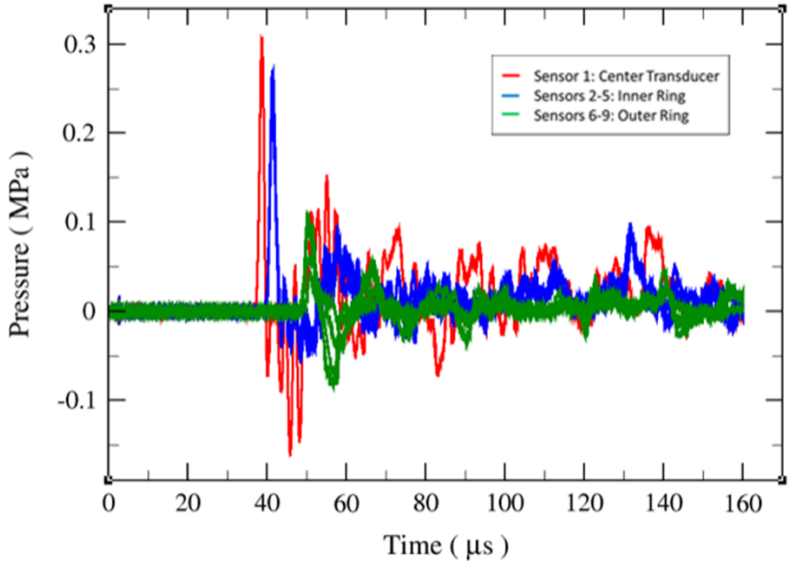

Figure B26. Pressure transducer results for the small spherical cavity (Happy)

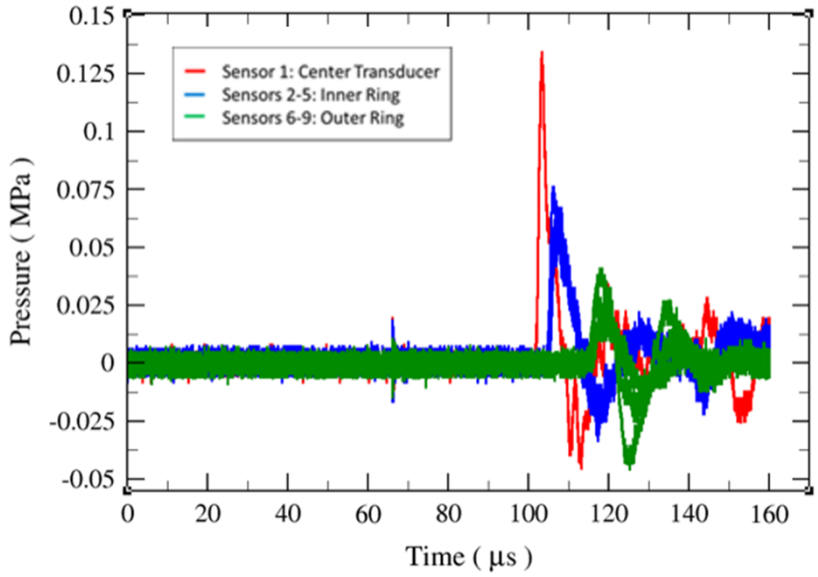

Figure B27. Pressure transducer results for the large hemispherical cavity (Mario)

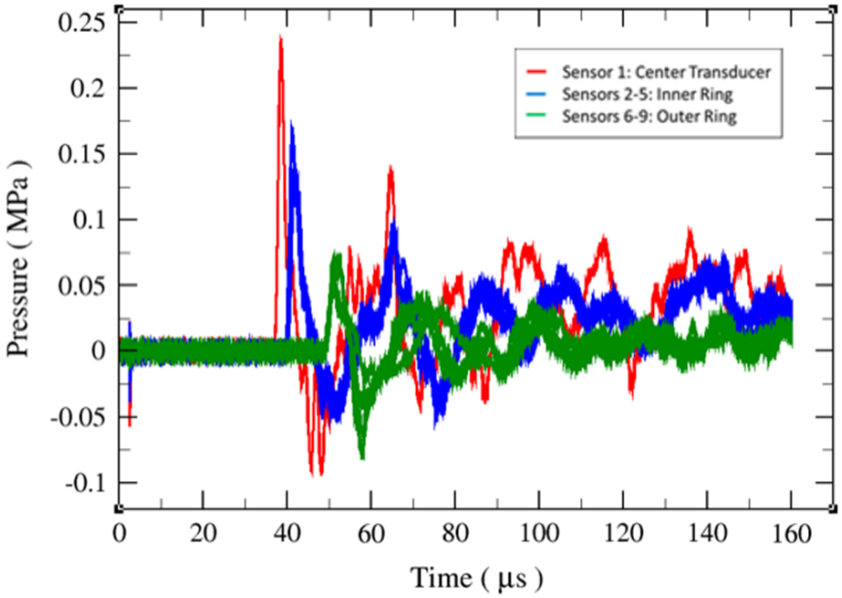

Figure B28. Pressure transducer results for the medium hemispherical cavity (Hamy)

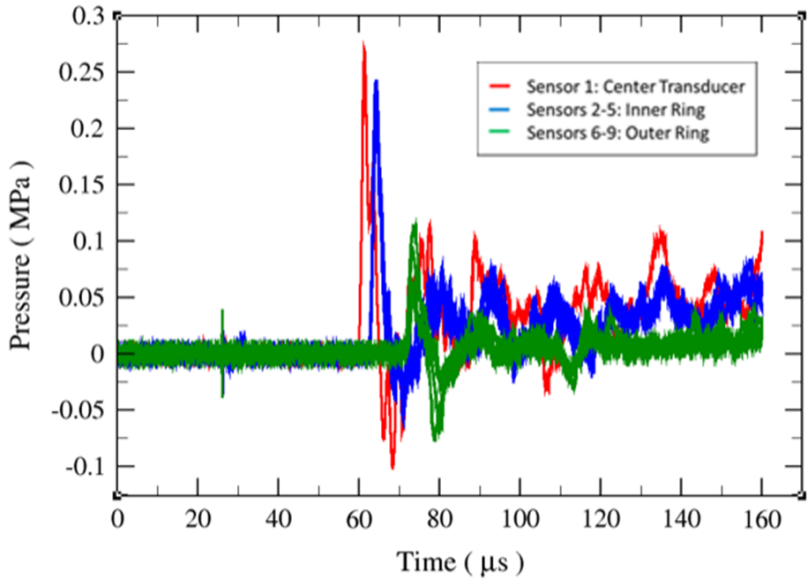

Figure B29. Pressure transducer results for the small hemispherical cavity (Luna)

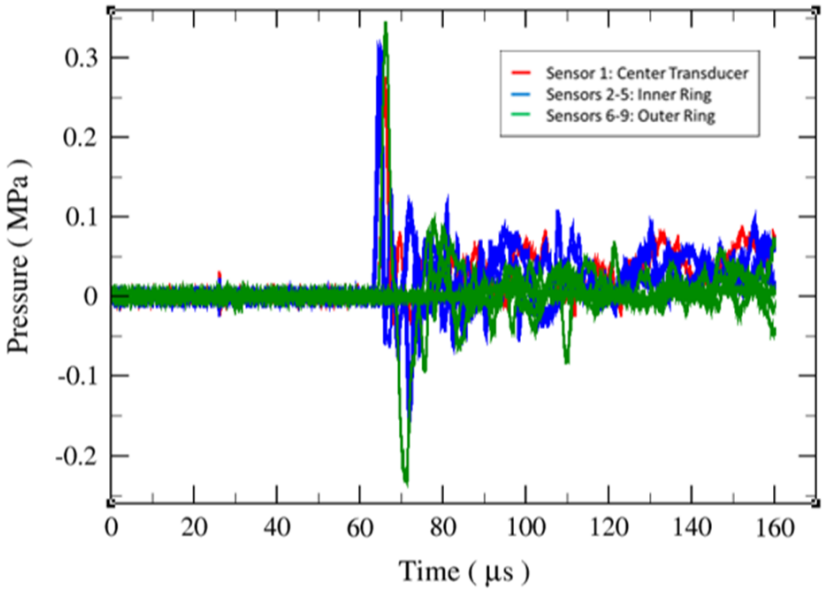

Figure B30. Pressure transducer results for the single-exit, small-diameter pipe cavity (Lambda)

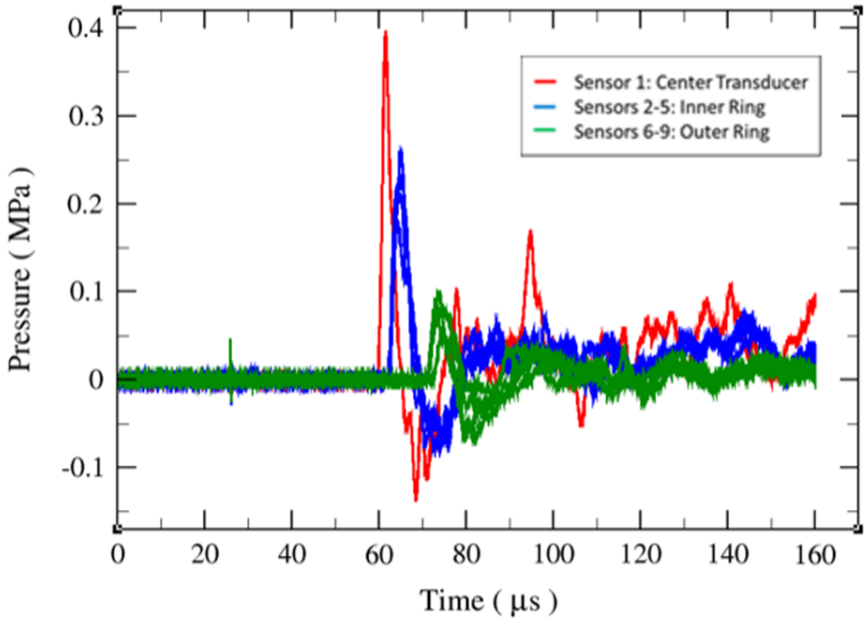

Figure B31. Pressure transducer results for the horizontal ovoid cavity (Hermione)

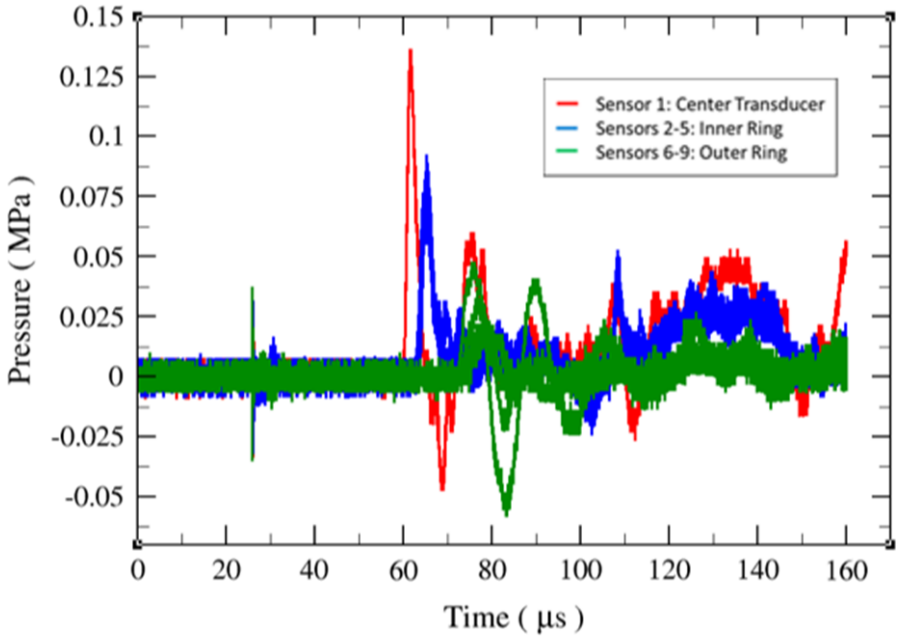

Figure B32. Pressure transducer results for the medium square (Draco)

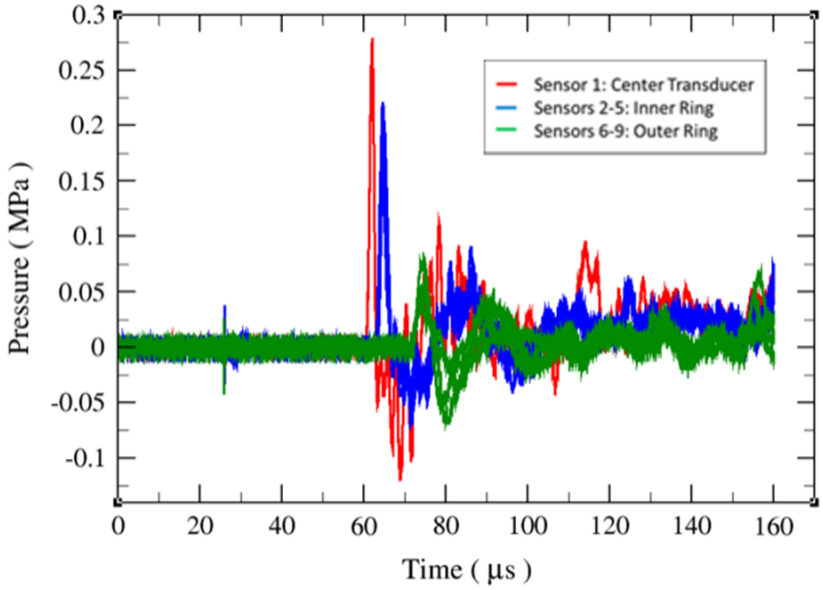

Figure B33. Pressure transducer results for the vertical ovoid (Ron)

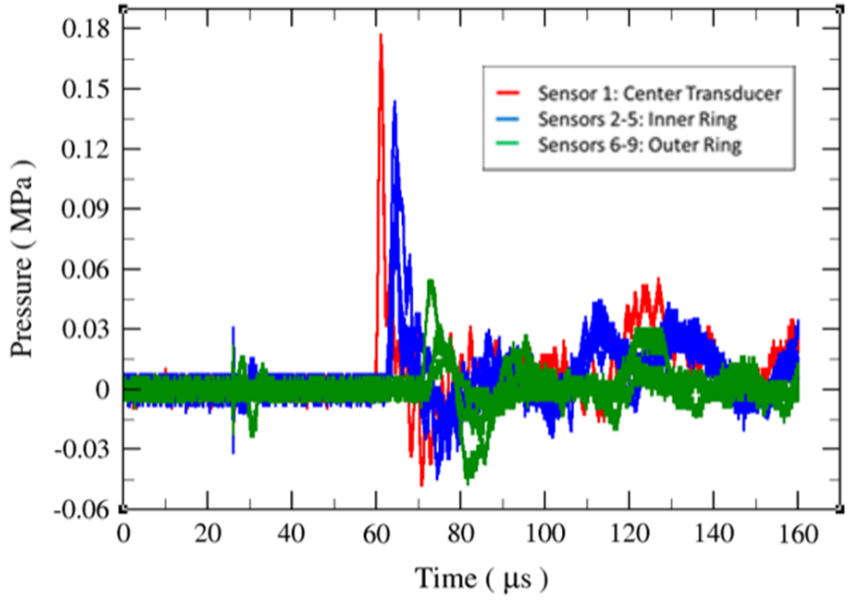

Figure B34. Pressure transducer results for the nonsymmetric cavity (Pumpkin)

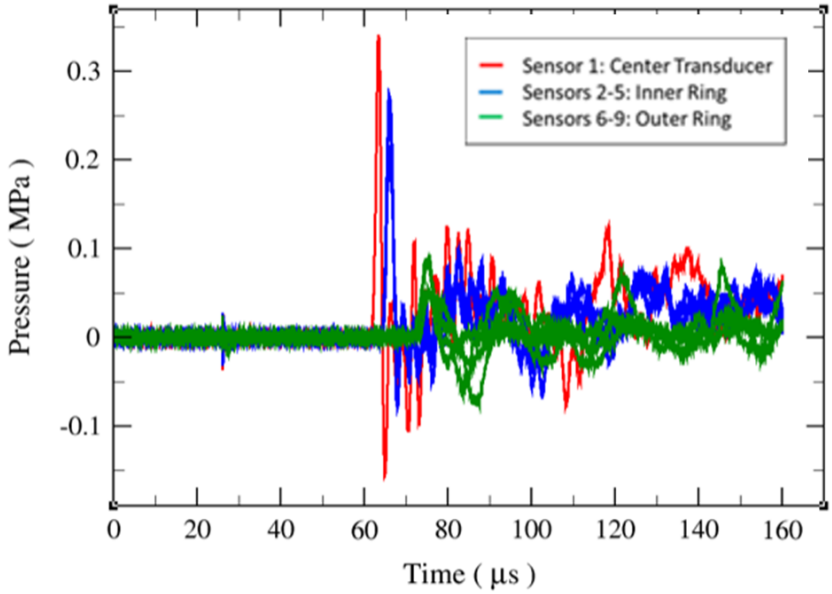

Figure B35. Pressure transducer results for the dual exit, small diameter pipe cavity (Tau)

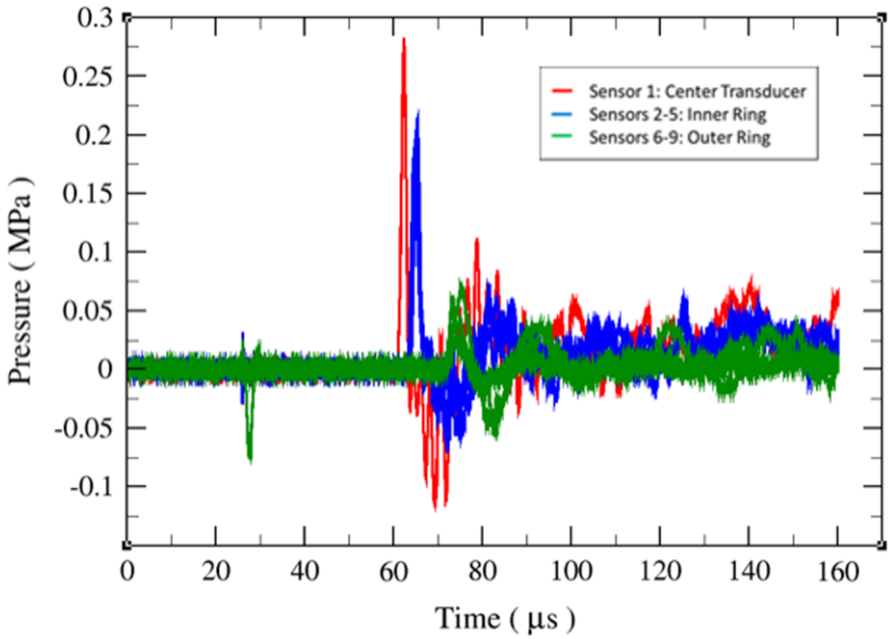

Figure B36. Pressure transducer results for the dual exit, large diameter pipe cavity (MrT)

REFERENCES

[1] Chojnicki, K., Cooper, M. and S. Guo "Laboratory measurements of shock propagation through spherical cavities in an optically accessible polymer," Sandia National Laboratories, SAND2017-12145, November 2017.

This page left blank

DISTRIBUTION

Email—Internal

Name	Org.	Sandia Email Address
Technical Library	01911	sanddocs@sandia.gov

Sandia National Laboratories

Sandia National Laboratories is a multimission laboratory managed and operated by National Technology & Engineering Solutions of Sandia LLC, a wholly owned subsidiary of Honeywell International Inc. for the U.S. Department of Energy's National Nuclear Security Administration under contract DE-NA0003525.